INTERNATIONAL JOURNAL OF AUTOMOTIVE AND MECHANICAL ENGINEERING
ISSN: 2229-8649 e-ISSN: 2180-1606
VOL. 20, ISSUE 4, 2023, 10850 – 10861
DOI: https://doi.org/10.15282/ijame.20.4.2023.04.0840

RESEARCH ARTICLE

Eigenfrequency Shift of Piezoelectric Backplate in Vibro-Acoustic Energy Harvesting

M.H. Mansor, M.S.M. Sani, and M.F. Hassan

Faculty of Mechanical and Automotive Engineering Technology, Universiti Malaysia Pahang, 26600 Pahang, Malaysia

ABSTRACT - Noise is increasingly recognised as a serious, worldwide public health concern. Noise is a type of occupational hazard that can cause damage to hearing and other health effects in workers who are exposed to high levels of noise in their work environment. Traditionally, noise can be controlled and suppressed but recently, noise can be useful and converted into electrical energy. The process of converting noise or acoustic waves into electrical energy by using a quarter wavelength resonator tube embedded with a flexible piezoelectric backplate was used in this study. The results show the maximum output voltage of 1.41 V/Pa at 112 Hz and 0.44 V/Pa at 225 Hz in the experiment, and 1.44 V/Pa at 106 Hz and 0.41 V/Pa at 226.5 Hz with incident sound waves at 90 dB. A parametric study was then performed by adjusting the lumped pointed mass at the piezoelectric backplate to tune the resonant frequencies of the system and the optimal power output. The point mass has given significant change in the acoustic properties. The maximum output power increased from 20.4 $\mu W/Pa^2$ at 112 Hz using a flexible back plate to 711 $\mu W/Pa^2$ at 119.75 Hz. Various small power applications can benefit from the approach by reducing and absorbing specific low-frequency bandwidths of continuous noise in the environment.

ARTICLE HISTORY
Received : 30th Nov. 2022
Revised : 15th Apr. 2023
Accepted : 16st Nov. 2023
Published : 26th Dec. 2023

KEYWORDS
Acoustic energy harvester;
Vibro-acoustic;
Eigenfrequency shift;
Piezoelectric;
Backplate.

1.0 INTRODUCTION

Over the past century, noise study has dramatically increased, which has been utilised and manipulated by converting it into another valuable energy such as electrical power. A work environment with high noise levels can be hazardous to the worker and cause damage to hearing and other health effects. This dangerous situation allows previous researchers to manipulate and convert noise or acoustic energy into electrical energy [1]–[8]. A developing field of study called acoustic energy harvesting (AEH) is being pursued to turn acoustic waves into valuable electrical energy. Without the use of batteries or other external power sources, this technique offers the potential to operate a variety of low-power gadgets, such as wireless sensors, implants, and wearable electronics [9], [10]. Acoustic energy, which is present in our daily lives and surroundings, has gone unnoticed as green energy that may be harvested, produced, and used without materially harming the environment [11]–[13]. Sound waves have a lower energy density and can only be captured in boisterous conditions; hence, AEH is less common than other energy harvesting techniques. Although specific applications have modest energy requirements, monitoring noise levels is essential to prevent noise pollution [14]–[17]. For example, in the case of a power plant, the employment of AEH devices can increase the efficiency of their equipment. Power plants will have low pollution levels because they will capture the noise emitted from their main components. This would enable nations to maintain high industrial output while reducing the number of by-products released into the ozone layer. It benefits the environment and boosts productivity across the board for the energy industry [18]–[20].

Commercially mature energy harvesting technologies, such as solar, wind, and hydro, are being developed to supply machines on a medium to large scale [17], [21]. Power consumption must be scaled down for small or devices less than 1 cm^3 to accommodate the devices' low power needs, and energy harvesting is employed as an alternate choice to replace primary and traditional power sources [21]–[23]. Low-power devices have evolved as powerful platforms for microelectromechanical system (MEMS) devices, wireless sensor networks, and compact health monitoring devices, as they are ecologically benign [24]–[27]. As a result, these type of devices that can work efficiently with low power density energy sources such as ambient noise has various advantages, most notably by prolonging the device's lifespan and decreasing the need for frequent battery changes. However, it's important to note that the efficiency of energy harvesting from low-power density sources may vary based on the specific technology and the environmental conditions in which the devices are deployed. As a consequence, acoustic energy harvesting research is vital and has the potential to expand in the future. Acoustic energy harvesting is defined as the technique of collecting continuous acoustic waves from the environment using an acoustic resonator tube and converting them into electrical energy using a transducer mechanism [3], [16], [28]. As acoustic waves propagate longitudinally in the medium element, an acoustic resonator tube is required to magnify the incident acoustic wave at a specific frequency, and standing resonant waves within the resonator stimulate the transducer mechanism [6], [8], [16], [29]. An acoustic resonator is typically employed to attenuate or insulate noise sources produced. Furthermore, it can also be built as an energy harvesting device to maximise the acoustic source rather than dissipate the sound energy in the tube.

*CORRESPONDING AUTHOR | M.H. Mansor | ✉ hatifi@ump.edu.my

Horowitz et al. [6] initially demonstrated a micromachine acoustic energy harvester based on an electromechanical Helmholtz resonator (HR) with a piezoelectric composite diaphragm made of lead zirconate titanate (PZT) affixed to the resonator chamber's end wall. It achieved a maximum output power of $0.34\ \mu W.cm^{-2}$ with an incident sound pressure level of 149 dB (referenced 20 Pa) at 13.6 kHz. Liu et al. [3] enhanced impedance matching by utilising a flyback converter and obtained $0.84\ mW.cm^{-2}$. Most previous studies focused on harvesting acoustic energy at relatively high frequencies ranging from a few hundred to kHz and MHz [1], [3], [4], [7], [8], [28], [30]–[32] using an HR as an acoustic resonator. Meanwhile, Bin, Li et al. [29], [33], [34] focused on low-frequency acoustic sources using multiple piezoelectric in the rigid quarter wavelength resonator. Bin Li developed a quarter wavelength resonator (QWR) array of several bimorph PZT plates and achieved a maximum power output of $57.4\ W.cm^{-2}$ at 100 dB (199Hz). Due to their lower spatial attenuation rates, sound sources in the typical life environment include a higher proportion of low-frequency components than high-frequency sound [16], [29], [35]. In terms of the controlling device, a quarter wavelength resonator is more suitable to control and amplify the low-frequency acoustic source. Previous researchers mainly investigated a decoupled model of an AEH system, in which the resonator system and transducer mechanism were examined separately. Less of them were concerned about the acoustic characteristic of the resonator that was used to excite the energy converter because the uncertainty of acoustic behaviour when the tube parameter and design changed.

The purpose of this study is to investigate the effect of a lumped point mass on the piezoelectric backplate on a fully-coupled acoustic energy harvesting (AEH) model in order to better understand the behaviour of the multiphysics system. Beginning with a fully-coupled numerical analysis of an AEH system using a QWR with a piezoelectric transducer patch put on the resonator's flexible back plate, finite element software is used to illustrate the results. The adjustable PZT backplate is implemented at the end of the QWR as an energy converter for optimisation, and a method is provided to regulate the structural and mechanical resonance of the flexible PZT backplate to the acoustic resonance of the QWR tube. The set of lumped point mass will be added at the middle of the PZT backplate and produce the output from the AEH mechanism. The numerical analysis will be compared to experimental analysis with the same condition.

One of the challenges in AEH is that sound waves have a wide frequency range, and different frequencies require different types of transducers to convert them into electrical energy. Several studies have explored ways to harvest energy across a wide frequency range, including broadband transducers and multi-stage energy harvesting systems. This paper concentrates on the frequency shift, whether it can be correlated or produce two dominant peak outputs for the energy harvesting system.

2.0 QUARTER WAVELENGTH RESONATOR TUBE WITH EMBEDDED PIEZOELECTRIC PATCH

A resonator tube is a device composed of an arrangement of elements whose acoustical reactance cancels at a specific frequency determined by the size of the resonator tube. It is frequently employed as a passive acoustic control or, in another interpretation, to remove undesired frequency elements from an acoustic system. Furthermore, an acoustic resonator tube can increase acoustic pressure at its resonance frequency [36]–[38]. Helmholtz and QWRs are two well-known resonators that have been extensively researched for acoustic applications [38], [39]. A third form of resonator, which is a half-wavelength resonator, has also been invented in recent years to provide acoustic dampening [36], [38], [40]. Chae et al. [41] compared the effectiveness of all three resonators using a half-wavelength resonator as a baseline. The evaluation demonstrated that compared to the other two resonators, the QWR had the highest efficiency of AEH [5], [41].

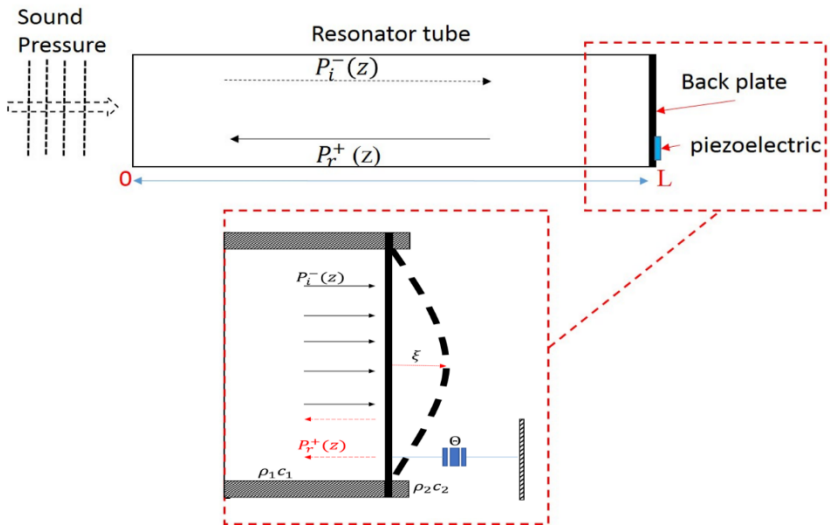

Figure 1. A sound pressure propagated into the L length of a QWR tube and reflected at the flexible backplate. The figure in the red dotted box represents the flexible backplate with piezoelectric embedded in the diaphragm system

Figure 1 shows a harmonic sound pressure $P(z) = P_0\, e^{-i\omega t}$ applied at the inlet of a rigid AWR tube, with the sound pressure propagating in the z direction, and it can be expressed as follows:

$$\left.\begin{aligned} \boldsymbol{p(z)} &= \boldsymbol{P_i e^{-ikz} e^{i\omega t}} \\ \boldsymbol{u(z)} &= \boldsymbol{\frac{P_i}{\rho_0 c} e^{-ikz} e^{i\omega t}} \end{aligned}\right\} \boldsymbol{for\ z > 0} \tag{1}$$

$$\left.\begin{aligned} \boldsymbol{p(z)} &= \boldsymbol{P_r e^{ikz} e^{i\omega t}} \\ \boldsymbol{u(z)} &= \boldsymbol{\frac{P_r}{\rho_0 c} e^{ikz} e^{i\omega t}} \end{aligned}\right\} \boldsymbol{for\ z < 0} \tag{2}$$

where p and u are the pressure and velocity of the air in the tube with the L length, respectively; ρ_0 is the equilibrium air density; $k = {}^{\omega}/_{c_0}$ is the wave number; and c_0 is the wave speed. P_i is the incident pressure and P_r is the reflected pressure, and both are complex amplitudes. The solution of the wave equation for the total pressure and velocity inside the tube is:

$$\boldsymbol{p(z) = P_i e^{-ikz} e^{i\omega t} + P_r e^{ikz} e^{i\omega t} = P e^{i\omega t}} \tag{3}$$

$$\boldsymbol{u(z) = \frac{P_i}{\rho_0 c} e^{-ikz} e^{i\omega t} - \frac{P_r}{\rho_0 c} e^{ikz} e^{i\omega t} = U e^{i\omega t}} \tag{4}$$

Based on Figure 1, if the boundary condition at z is equal to 0, Equation (3) becomes:

$$P_r = P_0 - P_i \tag{5}$$

The harmonic sound pressure $P(z) = P_0\, e^{-i\omega t}$ is applied at the inlet of the QWR tube and reflected. These two media are represented by the equilibrium air density inside the tube ρ_1 and sound of speed c_1, as well as air density on the other side of the backplate ρ_2 with the sound of speed c_2. Some sound pressure is transmitted through a flexible backplate and expressed as Equation (1). Equation (5) also applies to the boundary condition at $z = 0$, and the coefficients P_i *and* P_r are linked by the average particle velocity at the left-hand side of the backplate inside the tube, which moves with an average velocity equal to $j\omega\xi$. Hence, $z = L$.

$$u(L) = \frac{P_i}{\rho_1 c_1} e^{-ikL} e^{i\omega t} - \frac{P_r}{\rho_1 c_1} e^{ikL} e^{i\omega t} = j\omega\xi\, e^{i\omega t} \tag{6}$$

$$P_i e^{-ikL} - P_r e^{ikL} = j\omega\xi\rho_1 c_1 \tag{7}$$

where $P_{t2} = j\omega\xi\rho_2 c_2$. These fields are known as radiated fields. The total pressure field in the resonator tube is;

$$P^-(z) = P_i e^{-ikz} e^{i\omega t} + (P_0 - P_i) e^{ikz} e^{i\omega t} \tag{8}$$

The first term of Equation (8) representing the standing interference field is produced by the incidence and reflection from a complete backplate of the QWR. The second term represents the pressure field generated by backplate motion. Hence, the total field on the incident side equals the sum of the pressure field generated by the backplate and the radiated field. Accordingly, the total field on the right-hand side is reduced to the radiated field represented by the equation of motion of the backplate (i.e., piezoelectric), which can be written as:

$$\begin{cases} m\ddot{\xi} + \eta\dot{\xi} + s\xi + \Theta v = \dot{AP^-}(z) - AP^+(z) \\ \dfrac{v}{R} + C^s \dot{v} - \Theta\dot{\xi} = 0 \end{cases} \tag{9}$$

where A is the cross-section area of the backplate, ξ is the displacement of the mass m, v is the voltage across the resistor R, C^s is the piezoelectric capacitance, and Θ is the electromechanical coupling coefficient. Substituting the equation ($\xi = \xi e^{-i\omega t}$) and equation ($v = Ve^{-i\omega t}$) into Equation (9) produces:

$$\begin{aligned} \xi &= \frac{AP^-(z) - AP^+_{rad}(z)}{s - \omega^2 m + j\omega\eta + \dot{\Theta} V} \\ V &= \frac{\Theta R j\omega\xi}{1 + RC^s j\omega} \end{aligned} \tag{10}$$

The flexible backplate of the resonator can maximise the standing wave inside the resonator, and the piezoelectric can be embedded on the backplate in many ways without affecting the resonant frequency of the resonator tube. The previous researchers who used the resonator with a rigid backplate and attached piezoelectric inside the tube encountered a problem when altering the piezoelectric because the resonant frequency changed [16], [34]. The flexible backplate can be attached with one piezoelectric or several piezoelectrics that can increase the power output without affecting the resonator's resonant frequency.

2.1 Finite element analysis

A commercial finite element (FE) programme is utilised in this work to create a three-dimensional (3D) fully-coupled model of the proposed acoustic energy harvester. The model accounts for fluid-structure interaction and electromechanical connection. The QWR with a piezoelectric backplate inside the air domain constitutes the ultimately linked FE model. The resonator is a straight cylinder tube with one end open, and the other end closed by a flexible piezoelectric backplate. A piezoelectric transducer bond clamps the piezoelectric backplate circumferentially. The air domain is divided into three regions: one inside the resonator tube, one outside the resonator that generates a plane wave as a sound source, and another one is a more enormous spherical domain, a perfectly matched layer (PML). Figure 2 depicts the system's 3D and 2D models with the primary component.

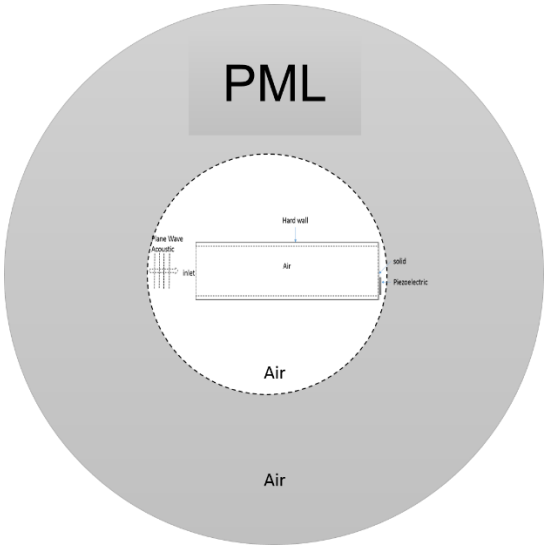

Figure 2. Fully-coupled FE model: (a) a 3D model that consists of the PML domain, plane wave source domain, and QWR

The system parameters are listed in Table 1.

Table 1. Geometric and material properties of the AEH system

Parameters	Values
QWR Tube:	
Diameter	100 [mm]
Length	735 [mm]
Wall Thickness	5 [mm]
Backplate:	
Diameter	100 [mm]
Length	4 [mm]
Backplate Properties:	
Young's Modulus (E)	0.84 [GPa]
Poisson's Ratio	0.35
Density ($\boldsymbol{\rho}$)	1,190 [kg/m^3]
Piezoelectric Patch Transducer:	
Length	37 [mm]
Width	18 [mm]
Thickness	0.5 [mm]
Piezoelectric Capacitance $(\boldsymbol{c_p})$	30.78 [nF]
Piezoelectric Density $(\boldsymbol{\rho_p})$	7,750 [kg/m^3]
Piezoelectric Young's Modulus $(\boldsymbol{E_p})$	30.36 [GPa]

Table 2. Geometric and material properties of the AEH system

Parameters	Values
Piezoelectric Relative Permittivity:	
$\varepsilon_{33}/\varepsilon_0$	1,750
$\varepsilon_{11}/\varepsilon_0$	1,650
Piezoelectric Charge Coefficient:	
d_{31}	-180
d_{33}	400
Room Temperature	15 [℃]
Air Density	1.2250 [kg/m^3]
Sound of Speed (c_0)	340.27 [m/s]

2.2 The finite element model boundary conditions

The PML is used as an absorbing and non-reflecting boundary. Although more memory and computational cost are required, PML is chosen because it describes sound radiation in an infinite domain. Figure 2 shows that the large spherical domain is the PML, whose particular radiation boundary condition only allows outgoing waves. The surrounding fluid for this global domain is air, and the QWR with a back plate embedded with a piezoelectric patch is in the global domain.

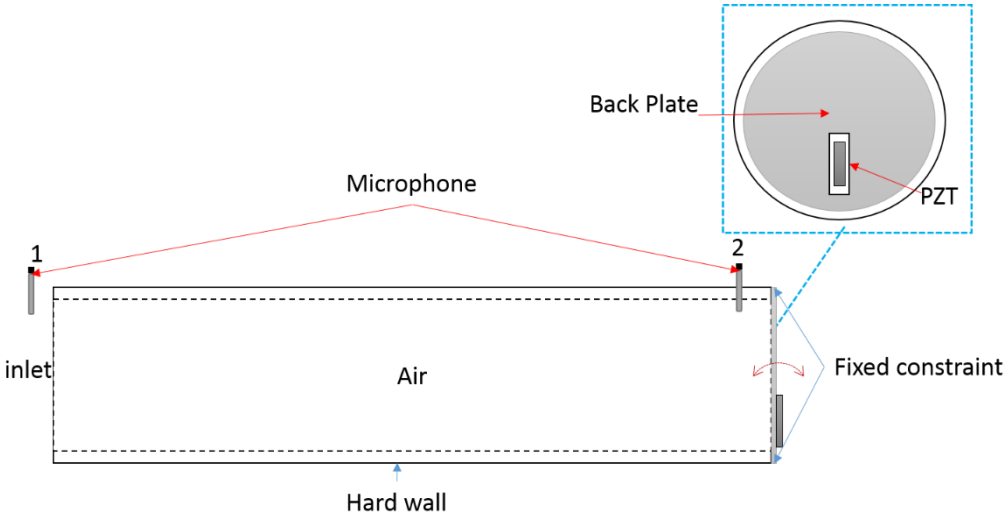

Figure 3. Boundary condition of the acoustic structure piezoelectric interaction for AEH

Figure 3 depicts the resonator's stiff construction, with the flexible acrylic backplate acting as a structure that interacts with the acoustic domain. A piezoelectric device of PZT-5 is placed in the rear plate at the optimal displacement location. The point mass is embedded in the middle of the PZT backplate. In order to simulate electrodes, the electrical boundary condition connects the voltage degree of freedom of the top and bottom surfaces of the piezo. The piezoelectric's top surface is an open circuit, while the bottom surface is grounded; the open circuit surface is then replaced with a resistive load to determine the voltage close circuit and power output. Microphone 1 measures acoustic pressure at the inlet ($p1$), while microphone 2 measures acoustic pressure at the resonator's end ($p2$). The damping element in the system is calculated experimentally and validated using FE analysis.

When modelling a wave problem, the computational mesh must give adequate wave resolution. This 3D acoustic model requires a minimum of six elements per wavelength when using second-order components (this is the default element for pressure acoustics). The acoustic model restricts the mesh's maximum element size.

$$L_{max} = \frac{\lambda_0}{6} \tag{11}$$

This translates to 0.25 m in this model. Consideration of the mesh within the PML is also necessary. It is advised that a sweeping mesh with six elements is used for the PML to dampen the outward waves appropriately. Meshing is critical for producing the best results in the shortest period. To prevent the solver from segregating the model, all domains are solved in the frequency domain using a sparse matrix direct solver like PARDISO and a direct fully-coupled solution. The PARADISO solver is based on the LU decomposition (i.e., lower and upper).

3.0 EXPERIMENTAL SETUP

The quarter wavelength resonator used an acrylic cylinder straight tube, and the backplate clamped at the end of the tube with piezoelectric was glued together with epoxy. Figure 4 depicts the schematic diagram of the AEH experimental setup. A chirp signal (frequency range of 50–250 Hz) from a data acquisition (DAQ) module (Signalcalc Ace Quattro) was boosted by a DIGITECH stereo power amplifier driver and fed into an RS 6 12-inch bass drive unit for an 8-ohm speaker. On the resonator, the speaker produced roughly 1 Pa incident sound pressure (p_incident). The incident sound pressure is amplified in the resonator and vibrates the backplate with a piezoelectric integrated. The acoustic pressure was measured using two microphones (model G.R.A.S 40PH CCP) at the intake ($p1$) and inside the resonator ($p2$). One microphone was placed 10 mm from the resonator's entrance, while the other was placed at the end of the resonator tube, 5 cm from the backplate. The DAQ module was used to assess various frequency responses measured and conditioned both microphones and the output voltage open circuit (VOC) generated by the lateral vibration of the backplate. Voltage with load resistance (VL) was calculated by connecting the PZT to the optimum resistive load and measuring the power output. Then, the PZT backplate introduced the lumped point masses for further investigation. The point was embedded at the backplate's centre, and the weight was changed for each experiment.

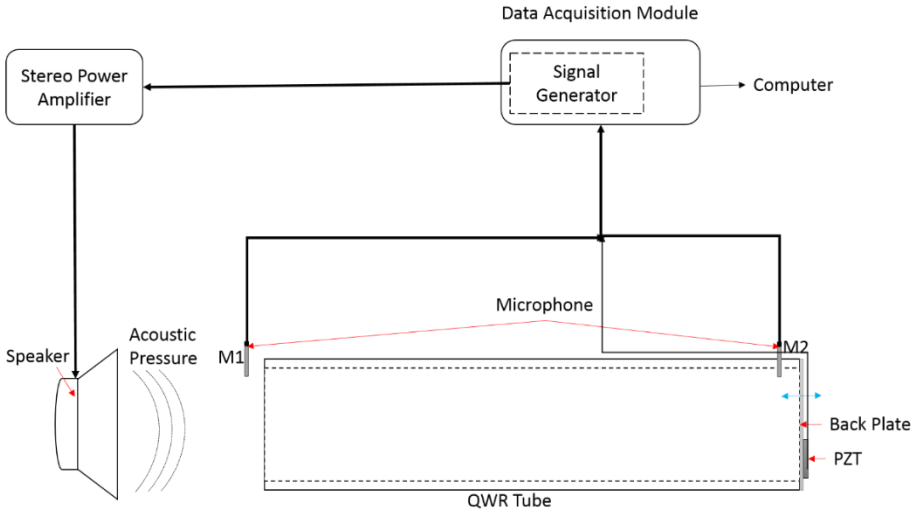

Figure 4. Schematic diagram of the experimental setup for AEH using a QWR and a flexible PZT backplate

4.0 EXPERIMENTAL RESULTS

4.1 Comparative study of the effect of additional point masses on the backplate

The previous analysis focused on the resonator with a bare backplate and a piezoelectric embedded in it. All the frequency response results are a ratio of pressure at the inlet and inside the resonator, voltage output circuit (VOC), voltage at load resistance, and power to the pressure at the inlet, p_1, which matches well for both experimental and FE analysis. Figure 5 and Figure 6 show the results of the frequency response of the pressure ratio $\left({}^{p_2}/_{p_1}\right)$ and phase for experimental and FEA analysis, respectively. For this study, point masses were added at the centre of the backplate to shift the PZT backplate resonance frequency and match it with the acoustic resonance frequency. Another technique to match the resonance frequency is using a backplate with a different thickness, which will affect the power output of this AEH system. The amplitude of the output decreases when the thickness of the backplate increases, which affects the maximum displacement of the PZT at the backplate. Figure 5 and Figure 6 show the effect of additional point masses on a bare backplate with a piezoelectric patch embedded in it.

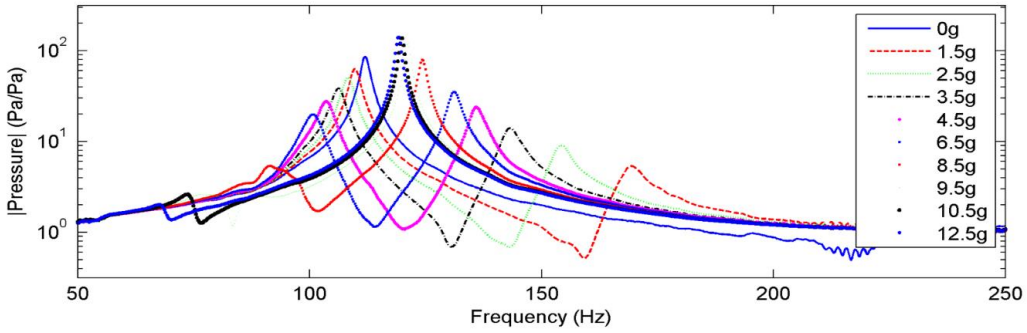

Figure 5. Experimental results for the frequency response of acoustic pressure inside the resonator $\left({}^{p_2}/_{p_1}\right)$ for nine additional masses: Magnitude and phase

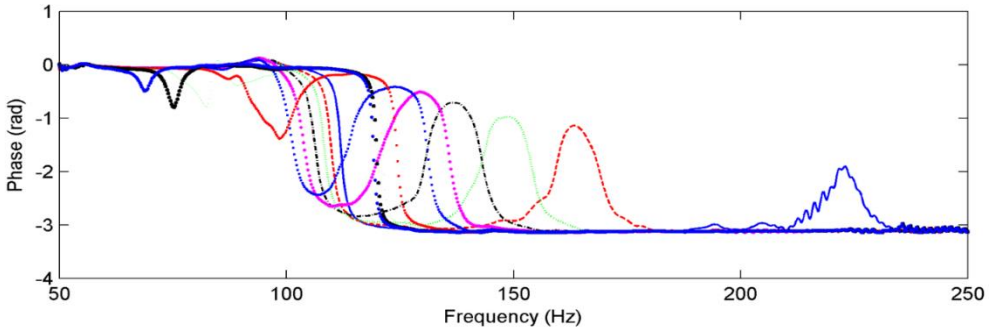

Figure 5. (Cont.)

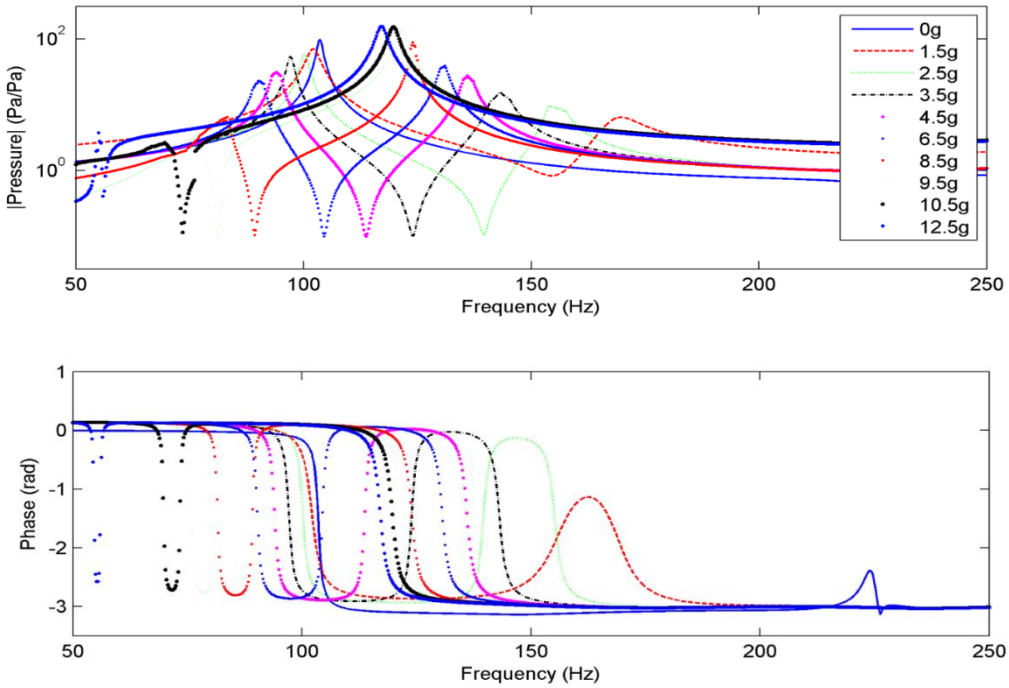

Figure 6. FEA results for the frequency response of acoustic pressure inside the resonator $\left({}^{p_2}/_{p_1}\right)$ for nine additional masses: Magnitude and phase

The comparative study involves the results from the bare backplate and the backplate with additional masses. Figures 5 and 6 match the frequency response function and phase response well. Then, the set of masses introduced on the PZT backplate, the FRF and the phase response for both figures show that the standing wave (f_1) and backplate resonant frequency (f_2) had shifted. As shown from the figures above, the effect of the additional mass on the PZT backplate, the magnitude peaks for both resonant frequencies shift and change. Interestingly, these figures for both analyses show that the resonant frequency of the backplate changes if the mass varies like theoretical [42]. Mass and the resonant frequency had a significant positive correlation[43]. Overall point mass affected both condition amplitude resonant frequency and eigenfrequency.

Figure 7(a)–(c) shows the summarised plot of resonant frequencies, the peak magnitude of pressure ratio, and VOC for the bare backplate and each additional point mass. The results are caused by the alteration of the backplate weight and acoustic resonance due to the additional masses on the backplate midpoint of the resonator. Interestingly, this correlation is related to the additional mass, whereas the mass increases the resonant frequency for both peaks, (f_1) and (f_2) decreases.

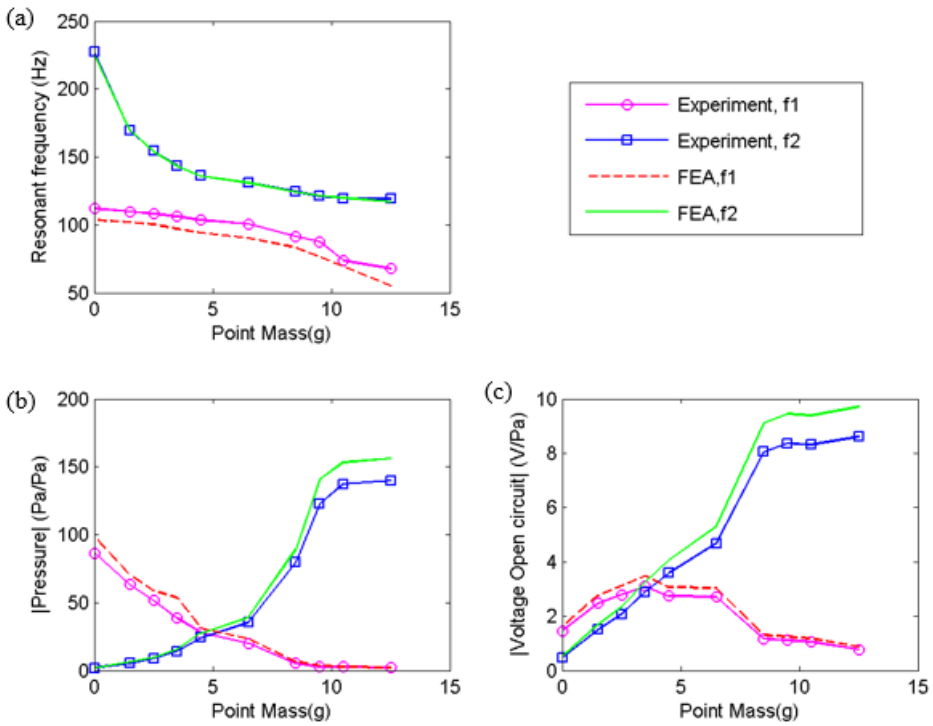

Figure 7. Experimental and FEA results for two frequencies at different point masses: (a) resonant frequencies for each point mass, (b) pressure ratio $(^{p_2}/_{p_1})$, and (c) VOC

Figure 7(a) shows clearly the presence of additional mass effect in the simulation and experimental of the resonant frequencies for (f_1) and (f_2). The single most striking observation to emerge from the figure was (f_2) shows a clear decreasing pattern. Furthermore, the presence of the piezoelectric inside the resonator [34], [44], [45], which can change the acoustic resonant frequency, and the additional masses on the backplate can also shift the resonance frequencies of the resonator and backplate. Due to this behaviour, the structure's resonant frequencies can be tuned close to each other through these additional point masses without affecting other parameters. The more surprising correlation is related to end correction, known as invisible acoustical length. When this length changes, the resonator tube's resonant frequency will shift.

The data in Figure 7 shows that the flexible backplate's impact has a significant influence. Figure 7(b) presents the plot of pressure ratio peaks at each point mass for both resonant frequencies. A comparison of the two frequencies reveals that (f_1) decreases while (f_2) increases when additional masses are added at the midpoint of the backplate. Very little was found in the literature on the effect of extra mass presence in the acoustic resonator backplate. Furthermore, the amplitude peak appears to have the same value at 4.5 g point mass, which is a clear benefit to the AEH system so that it can produce broadband frequency. Figure 7(c) illustrates the peak values of the ratio of the VOC to the pressure at the inlet (p_1) for each additional mass. The trend of the plot is similar to the pressure ratio. If the system masses further increase for both modes, the value of VOC will decrease after the maximum value at the optimum additional mass. From the results in Figure 7(b), the acoustic pressure inside the tube has a higher amplitude at 0 g, 4.5 g and 12.5 g point mass either for (f_1) or (f_2). This results data shows that two frequencies resonant have a significant role in exciting the backplate at the higher velocity to produce optimum power output.

4.2 Acoustic pressure inside the tube

As can be seen from the figure above, the three additional masses that significantly impact AEH output are presented in Figure 8(a)–(d). The figure shows three set masses of the frequency response of acoustic ratio pressure, $(^{p_2}/_{p_1})$ and the phase at the end of the back plate. The three sets of data for no mass, 4.5 g and 12.5 g are chosen based on standing wave and resonant frequency peak. In Figure 8 there is a clear trend of increasing the output value for both resonant frequency while 4.5 g mass show the potential of broadband frequency for output. These resonant frequencies are used to excite the PZT backplate of the AEH system.

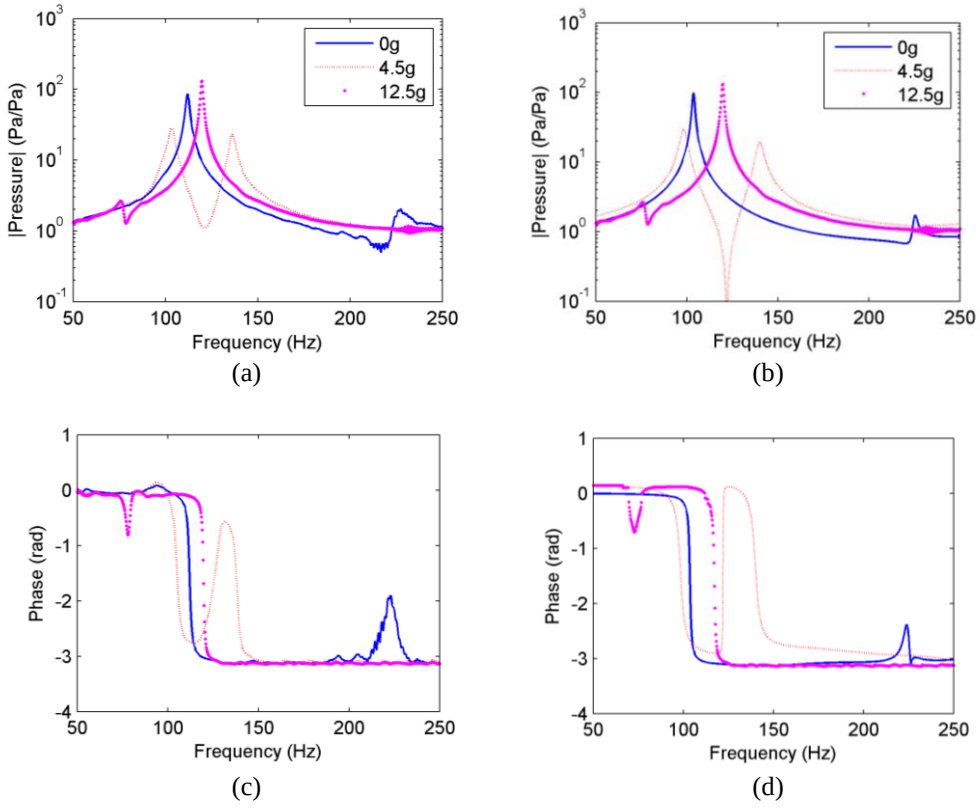

Figure 8. Frequency response of pressure ratio (p_2/p_1): experimental results of (a) magnitude and (b) phase and FEA results of (c) magnitude and (d) phase

Based on Figure 8(a)–(d), Table 2 summarises the effect of additional point masses on the backplate and compares it with the bare backplate results. Figure 8(b) and (d) show the phase for each mass that shifted based on the resonance frequency of the AEH system. As Table 2 shows, there is a significant difference between the data set regarding the natural frequency and amplitude value.

Table 2. Experimental and FEA results for additional masses on the QWR backplate

Mass	Mode	Experiment		FEA	
		Natural Freq (Hz)	Peak (Pa/Pa)	Natural Freq (Hz)	Peak (Pa/Pa)
0 g	f_1	112	86	104	96
	f_2	226.75	1.9	225.5	1.75
4.5 g	f_1	103.5	28.38	98.25	29.61
	f_2	136	23	139.8	20
12.5 g	f_1	75.5	2.63	70	2.7
	f_2	119.8	131.2	120	132

As shown in Table 2, the results indicate that the resonance frequency of the acoustic energy harvester system shift, where the bare backplate with 0 g mass shows two peaks at 112 Hz and 226.75 Hz. Meanwhile, 4.5 g masses show that the system's second eigenfrequency shifted from 228 to 136 Hz, and the first eigenfrequency shifted from 112 to 103.5 Hz. The highest acoustic pressure frequency response peak for 4.5 g masses is 28.38 (Pa/Pa) at 103.5 Hz and close to the second peak at 28.38 (Pa/Pa). For the 12.5 g additional masses, the first resonant frequency (f_1) the 4.5 g masses shifted to 75.5 Hz, and the second resonant frequency shifted to 119.8 Hz. The 12.5 g additional masses on the backplate produced the highest acoustic pressure at the back plate of 131.2 (Pa/Pa) compared to the 4.5 g masses (28.38 (Pa/Pa)) and the bare backplate (86 (Pa/Pa)). There was a significant positive correlation between the resonant frequency and additional mass, and the amplitude value produced optimum output. The added mass strongly contributed to the AEH system regarding optimum production and flexible eigenfrequency.

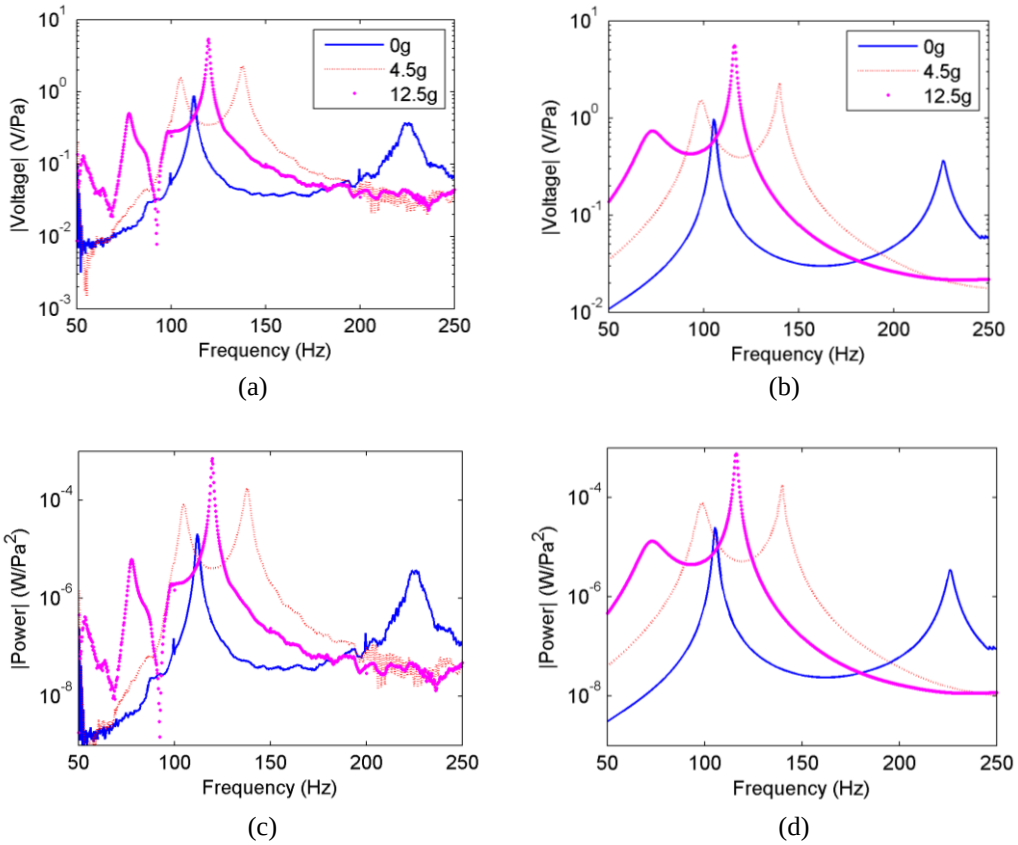

Figure 9. Frequency response of VL to the pressure at inlet ratio $\left({}^{VL}/_{p_1}\right)$ and power to the pressure at the inlet $\left({}^{Power}/_{{p_1}^2}\right)$: (a) experimental VL (b) FEA VL, (c) experimental power, and (d) FEA power

Figure 9(a)–(d) shows the voltage at optimum load resistance (VL) for the bare backplate, 4.5 g, and 12.5 g additional masses. The optimum resistive load for the 0 g backplate is 36 $k\Omega$. Meanwhile, for a backplate with the 4.5 g additional masses, the optimum resistive load is 32 $k\Omega$, and for the 12.5 g additional masses, the optimum resistive load is 40 $k\Omega$. Figure 9(c) and 9(d) show the optimum output power of three different additional masses at the backplate obtained from the measured voltage at optimum resistive load using the equation ${}^{V^2}/_{R_{optimum}}$. The figures show that the optimum power output for the flexible bare back plate increased when additional masses were introduced into the system. The optimum output power generated from the 12.5 g additional masses is around 711 $\mu W/Pa^2$ at 119.8 Hz compared to the bare backplate that produced power of approximately 20.2 $\mu W/Pa^2$ at 112 Hz. The 4.5 g additional masses generated the output power of 80.2 $\mu W/Pa^2$ at 103.5 Hz and 174 $\mu W/Pa^2$ at 136 Hz. The maximum output power increased after adding the masses to the flexible PZT back plate, and the resonance frequency shifted in the AEH system.

In this figure, the quality factors of the 4.5 g additional masses on the backplate are 28 (ζ~0.018) and 41 (ζ~0.0123). This condition is due to the significant decrease in the output voltage and acoustic pressure at the second set when aligning the resonance frequency of the flexible PZT back plate. As a result of adding additional masses at the PZT back plate to improve the AEH system, the 12.5 g additional masses have a significant effect by increasing the quality factor and producing the optimum value of VL and power for the energy harvesting system. On the other hand, the quality factors of the 12.5 g masses acoustic energy harvester are 26 (ζ~0.019) and 102 (ζ~0.0049). However, this result has not previously been described.

5.0 CONCLUSIONS

This study set out to determine the effect of additional point mass presence in the fully coupled simulation and experiments of an AEH mechanism using a QWR tube with a piezoelectric back plate. The numerical analysis in this study was carried out using COMSOL Multiphysics. This QWR energy harvesting mechanism harvested acoustic energy at a low frequency (around 50–250 Hz) with an incident pressure wave of 90 dB. The piezoelectric back plate generated VOC around 1.88 V/Pa at 106.5 Hz and 0.75 V/Pa at 224 Hz compared to the experiment with 1.73 V/Pa at 112 Hz and 0.36 V/Pa at 228 Hz. Meanwhile, the power dissipated in the resistor for the experiment is 20.4 $\mu W/Pa^2$ at 112 Hz and 3.6 $\mu W/Pa^2$, and the simulation reached a maximum of 24.2 $\mu W/Pa^2$ at 106.5 Hz and 6.87 $\mu W/Pa^2$ at 228 Hz. The investigation of additional masses at the back of the PZT backplate has shown that it increased the power output at optimum resistive load for the AEH system. The resonant frequency of the QWR tube shifted proportionally to the added masses on the back plate with the piezoelectric embedded. Moreover, the improved power output, voltage, and acoustic

pressure at the end of the resonator tube also increased. The output power increased from 20.4 $\mu W/Pa^2$ at 112 Hz using a flexible back plate to 711 $\mu W/Pa^2$ at 119.75 Hz for the 12.5 g additional masses. Based on the results, acoustic energy harvesting using the QWR with the PZT back plate and 12.5 g additional masses produced optimum power output experimentally and was validated by numerical analysis. By implementing a QWR with a flexible backplate, piezoelectric can be embedded on the backplate in many ways and quantities without affecting the resonator's resonance frequency. It's important to note that the effects of adding mass to a quarter-wavelength resonator depend on various factors, including the specific design, the material of the backplate, and the intended application. This work provides additional evidence concerning the main study, the vibroacoustic energy harvesting system.

6.0 ACKNOWLEDGEMENT

The authors would like to be obliged to Advanced Structural Integrity and Vibration Research Group (ASIVR), Universiti Malaysia Pahang Al-Sultan Abdullah, for providing laboratory facilities and financial assistance under project grant no. RDU230339.

7.0 REFERENCES

[1] Y. Tomimatsu, H. Takahashi, T. Kobayashi, K. Matsumoto, T. Itoh, and R. Maeda, "A piezoelectric cantilever with a Helmholtz resonator as a sound pressure sensor," *Journal of Micromechanics and Microengineering*, vol. 23, no. 11, p. 114003, 2013.

[2] Y. Wang, X. Zhu, T. Zhang, S. Bano, H. Pan, L. Qi, Z. Zhang, and Y. Yuan, "A renewable low-frequency acoustic energy harvesting noise barrier for high-speed railways using a Helmholtz resonator and a PVDF film," *Applied Energy*, vol. 230, pp. 52–61, 2018.

[3] F. Liu, S. Horowitz, T. Nishida, L. Cattafesta, and M. Sheplak, "A multiple degree of freedom electromechanical Helmholtz resonator," *Journal of the Acoustical Society of America*, vol. 122, no. 1, pp. 291–301, Jul. 2007.

[4] T. Zaid, S. Saat, N. Jamal, S. H. Husin, Y. Yusof, and S. K. Nguang, "A development of acoustic energy transfer system through air medium using push-pull power converter," *WSEAS Transactions on Power Systems*, vol. 11, pp. 35-42, 2016.

[5] B. Li and J. Ho You, "Simulation of acoustic energy harvesting using piezoelectric plates in a quarter-wavelength straight-tube resonator," *In Proceedings of the 2012 COMSOL Conference*, Boston, 2012.

[6] S. B. Horowitz, M. Sheplak, L. N. Cattafesta, and T. Nishida, "MEMS Acoustic Energy Harvester," *Journal of Micromechanics and Microengineering*, vol. 16, no. 9, S174, 2006.

[7] K. Ma, T. Tan, Z. Yan, F. Liu, W. H. Liao, and W. Zhang, "Metamaterial and Helmholtz coupled resonator for high-density acoustic energy harvesting," *Nano Energy*, vol. 82, p. 105693, 2021.

[8] S. P. Matova, R. Elfrink, R. J. M. Vullers, and R. Van Schaijk, "Harvesting energy from airflow with a michromachined piezoelectric harvester inside a Helmholtz resonator," *Journal of Micromechanics and Microengineering*, vol. 21, no. 10, p. 104001, 2011.

[9] G. R. Ahmed Jamal, H. Hassan, A. Das, J. Ferdous, and S.A. Lisa, "Generation of Usable Electric Power from Available Random Sound Energy," *In 2013 International Conference on Informatics, Electronics and Vision (ICIEV)*, IEEE, pp. 1 – 4, 2013.

[10] A. J. Moradewicz and M. P. Kazmierkowski, "High efficiency contactless energy transfer system with power electronic resonant converter," *Bulletin of the Polish Academy of Sciences: Technical Sciences*, pp. 375-381, 2009.

[11] M. A. Pillai and E. Deenadayalan, "A review of acoustic energy harvesting," *International Journal of Precision Engineering and Manufacturing*, vol. 15, no. 5. pp. 949–965, 2014.

[12] J. Choi, I. Jung, and C. Y. Kang, "A brief review of sound energy harvesting," *Nano Energy*, vol. 56, pp. 169–183, 2019.

[13] D. Sun, Y. Xu, H. Chen, K. Wu, K. Liu, and Y. Yu, "A mean flow acoustic engine capable of wind energy harvesting," *Energy Conversion and Management*, vol. 63, pp. 101–105, 2012.

[14] K. F. Chen, J. Ho, and E. Yap, "Piezoelectric approach on harvesting acoustic energy," *International Journal of Energy and Power Engineering*, vol. 9, no. 8, pp. 774 – 780, 2015.

[15] A. B. Atrah and H. Salleh, "Simulation Of Acoustic Energy Harvester Using Helmholtz Resonator With Piezoelec-Tric Backplate," *In 20th International Congress in Sound and Vibration (ICSV20)*, pp. 30 -37, 2013.

[16] B. Li, J. H. You, and Y. J. Kim, "Low frequency acoustic energy harvesting using PZT piezoelectric plates in a straight tube resonator," *Smart Mater Struct*, vol. 22, no. 5, p. 055013, 2013.

[17] A. Erturk and D. J. Inman, *Piezoelectric Energy Harvesting*. John Wiley & Sons, United Kingdom, 2011.

[18] S. Noh, H. Lee, and B. Choi, "A study on the acoustic energy harvesting with Helmholtz resonator and piezoelectric cantilevers," *International Journal of Precision Engineering and Manufacturing*, vol. 14, no. 9, pp. 1629–1635, 2013.

[19] T. Zaid, S. Saat, N. Jamal, Z. Mustapa, Y. Yusmarnita, and S. K. Nguang, "A study on performance of the acoustic energy transfer system through air medium using ceramic disk ultrasonic transducer," *Journal of Applied Sciences*, vol. 16, no. 12, pp. 580 – 587, 2013.

[20] H. S. Kim, J. H. Kim, and J. Kim, "A review of piezoelectric energy harvesting based on vibration," *International Journal of Precision Engineering and Manufacturing*, vol. 12, no. 6, pp. 1129–1141, 2011.

[21] J. J. Sun, A. Hall, I. Simoneishvilli, E. K. Akdogan, and A. Safari, "Novel piezoelectric sensors and actuators," *In 3rd International Conference on Ceramic Interconnect and Ceramic Microsystems Technologies, CICMT 2007*, pp. 116 – 122, 2007.

[22] K. P. S. Adamu Murtala Zungeru, Li-Minn Ang, SRS. Prabaharan, "Radio Frequency Energy Harvesting and Management for Wireless Sensor Networks," in *Green Mobile Devices and Networks: Energy Optimization and Scavenging Techniques*, pp. 1–385, 2012.

[23] X. Zhang, H. Pan, L. Qi, Z. Zhang, Y. Yuan, and Y. Liu, "A renewable energy harvesting system using a mechanical vibration rectifier (MVR) for railroads," *Applied Energy*, vol. 204, pp. 1535–1543, 2017.

[24] P. Muralt, M. Marzencki, B. Belgacem, F. Calame, and S. Basrour, "Vibration Energy Harvesting with PZT Micro Device," in *Procedia Chemistry*, pp. 1191–1194, 2009.

[25] S. Du, Y. Jia, C. Zhao, S. T. Chen, and A. A. Seshia, "Real-world evaluation of a self-startup SSHI rectifier for piezoelectric vibration energy harvesting," *Sensors and Actuators A: Physical*, vol. 264, pp. 180–187, 2017.

[26] W. Yang and S. Towfighian, "A hybrid nonlinear vibration energy harvester," *Mechanical Systems and Signal Processing*, vol. 90, pp. 317–333, 2017.

[27] L. Gu, "Low-frequency piezoelectric energy harvesting prototype suitable for the MEMS implementation," *Microelectronics Journal*, vol. 42, no. 2, pp. 277–282, 2011.

[28] A. Yang *et al.*, "Tunable acoustic energy harvester using Helmholtz resonator and dual piezoelectric cantilever beams," in *IEEE International Ultrasonics Symposium, IUS*, IEEE Computer Society, pp. 2494–2497, 2014.

[29] B. Li, A. J. Laviage, J. H. You, and Y. J. Kim, "Harvesting low-frequency acoustic energy using multiple PVDF beam arrays in quarter-wavelength acoustic resonator," *Applied Acoustics*, vol. 74, no. 11, pp. 1271–1278, 2013.

[30] M. A. Pillai and D. Ezhilarasi, "Improved Acoustic Energy Harvester Using Tapered Neck Helmholtz Resonator and Piezoelectric Cantilever Undergoing Concurrent Bending and Twisting," in *Procedia Engineering*, Elsevier Ltd, pp. 674–681, 2016.

[31] X. Ji, L. Yang, Z. Xue, L. Deng, and D. Wang, "Enhanced quarter spherical Acoustic energy harvester based on dual Helmholtz resonators," *Sensors*, vol. 20, no. 24, p. 7275, 2020.

[32] S. Horowitz, T. Nishida, L. Cattafesta, and M. Sheplak, "Development of a micromachined piezoelectric microphone for aeroacoustics applications," *Journal of the Acoustical Society of America*, vol. 122, no. 6, pp. 3428–3436, 2007.

[33] B. Li and J. Ho You, "Comparison study of standard, conventional SSHI and self-powered SSHI interface circuits in piezoelectric energy conversion," in *ICAST2013: 24 th International Conference on Adaptive Structures and Technologies*, Aruba, 2013.

[34] B. Li and J. Ho You, "Enhanced output power by eigenfrequency shift in acoustic energy harvester," *In Active and Passive Smart Structures and Integrated Systems 2014*, vol. 9057, pp. 757-764, 2014.

[35] B. Li, A. J. Laviage, J. Ho You, and Y.-J. Kim, "Acoustic energy harvesting using quarter-wavelength straight-tube resonator," *Applied Acoustic*, vol. 74, no. 11, pp. 1271–1278, 2013.

[36] W. Pan, X. Xu, J. Li, and Y. Guan, "Acoustic damping performance of coupled Helmholtz resonators with a sharable perforated sidewall in the presence of grazing flow," *Aerospace Science and Technology*, vol. 99, p. 105573.

[37] L. Ning, Y. Z. Wang, and Y. S. Wang, "Active control of elastic metamaterials consisting of symmetric double Helmholtz resonator cavities," *International Journal of Mechanical Sciences*, vol. 153–154, pp. 287–298, Apr. 2019.

[38] A. Soto-Nicolas, "Measurements on Quarterwavelength Tubes and Helmholtz Resonators," *Journal of the Acoustical Society of America*, vol. 123, no. 5, p. 3842, 2008.

[39] T. A. Johansson and M. Kleiner, "Theory and experiments on the coupling of two Helmholtz resonators," *Journal of the Acoustical Society of America*, vol. 110, no. 3, pp. 1315–1328, 2001.

[40] K. S. Line, "Two Dimensional Open Channel Acoustic Resonator With Absorption," Research Report, University of Idaho, Moscow, 2008.

[41] C. H. Sohn and J. H. Park, "A comparative study on acoustic damping induced by half-wave, quarter-wave, and Helmholtz resonators," *Aerospace Science and Technology*, vol. 15, no. 8, pp. 606–614, 2011.

[42] V. Ondra and B. Titurus, "Theoretical and experimental modal analysis of a beam-tendon system," *Mechanical Systems and Signal Processing*, vol. 132, pp. 55–71, 2019.

[43] M. M. Hatifi, M. H. Firdaus, and A. Y. Razlan, "Modal analysis of dissimilar plate metal joining with different thicknesses using MIG welding," *International Journal of Automotive and Mechanical Engineering*, vol. 9, no. 1, pp. 1723–1733, 2014.

[44] B. Li and J. H. You, "Harvesting ambient acoustic energy using acoustic resonators," in *Proceedings of Meetings on Acoustics*, vol. 12, no. 1, p. 1, 2011.

[45] B. Li and J. Ho You, "Experimental study on self-powered synchronized switch harvesting on inductor circuits for multiple piezoelectric plates in acoustic energy harvesting," *Journal of Intelligent Material Systems and Structures*, vol. 26, no.13, pp. 1646-1655, 2015.